ADVANCING EARTH AND SPACE SCIENCES

Geophysical Research Letters

RESEARCH LETTER
10.1029/2025GL119706

Key Points:

- Earth system models with 2.8–10 km grid spacing represent trade-wind shallow mesoscale circulations and moisture co-variability
- Disabling deep and shallow convection parameterizations enhances shallow mesoscale circulations and increases their occurrence
- Convection parameterizations have a larger impact than ocean models on shallow mesoscale circulations

Supporting Information:

Supporting Information may be found in the online version of this article.

Correspondence to:

I. C. D. V. Dragaud,
iandragaud@lamma.ufrj.br;
ian.dragaud@uni-hamburg.de

Citation:

Dragaud, I. C. D. V., Vogel, R., Mellado, J. P., & Becker, T. (2026). Simulating shallow mesoscale overturning circulations in the trades with kilometer-scale Earth system models. *Geophysical Research Letters*, *53*, e2025GL119706. https://doi.org/10.1029/2025GL119706

Received 30 SEP 2025
Accepted 19 APR 2026

Simulating Shallow Mesoscale Overturning Circulations in the Trades With Kilometer-Scale Earth System Models

Ian C. D. V. Dragaud[1], Raphaela Vogel[1], Juan Pedro Mellado[1], and Tobias Becker[2]

[1]Meteorological Institute, University of Hamburg, Hamburg, Germany, [2]European Centre for Medium-Range Weather Forecasts (ECMWF), Bonn, Germany

Abstract Shallow mesoscale overturning circulations (SMOCs) are ubiquitous in the trades, primarily triggered by mesoscale convective heating and influencing the organization of shallow cumuli. Accurate representation of SMOCs and their co-variability with moisture is crucial for capturing mesoscale cloud organization in models and improving climate predictions. Coarse-resolution global climate models cannot resolve SMOCs, but multi-decadal scenario simulations with 10 km grid spacing motivate their use for assessing SMOC representation. At kilometer-scale resolutions, thermals of shallow convection are partially resolved, yet convective heating still relies on parameterizations for unresolved processes. Both finer grid spacing and convection schemes influence the magnitude and vertical distribution of shallow convective heating, controlling SMOC characteristics. Using EUREC^{4}A campaign data as reference, we show that models with 2.8–10 km horizontal grid spacing reproduce trade-wind shallow circulations and their co-variability with moisture. The findings highlight the importance of model configuration in accurately simulating the strength of mesoscale circulations.

Plain Language Summary Circulations confined to the lowest few kilometers of the atmosphere, with a horizontal size of around 100 km, are prevalent over the tropical oceans. These circulations are closely linked to changes in moisture and influence the amount and organization of shallow clouds. Representing these circulations in climate models is therefore important for improving predictions of climate. Traditional global models with coarse resolution cannot capture these features, but new simulations with finer resolutions (approximately 10 times finer) are now possible. Comparing these simulations with observations, this study shows that the evaluated models can reproduce the key features of shallow circulations and their link to moisture. The results also show how the configuration of a model influences its ability to represent these processes accurately.

1. Introduction

In the trade-wind boundary layer, surface-driven turbulent eddies generate small thermals that merge, widen, rise above the condensation level, and form shallow cumuli as moisture condenses (Bony et al., 2025). Trade-wind cumuli are ubiquitous in the tropical and subtropical marine boundary layer. These patchy and scattered clouds organize into a variety of patterns with characteristic length scales in the meso-β range, that is, on the order of 20–200 km (Stevens et al., 2019). Circulation-driven water vapor convergence likely develops mesoscale shallow convection patterns and convective heating at these scales drives vertical motion (Janssens et al., 2024), one of the main triggering mechanisms of shallow mesoscale overturning circulations (so-called SMOCs) (George et al., 2023).

SMOCs are prevalent in the trades, with typical horizontal scales on the order of 100 km, largely confined to the lowest ~2.3 kilometers of the atmosphere and extending down to the surface (George et al., 2023; Janssens et al., 2024). Descending branches of SMOCs occur in dry columns, while ascending branches are found in moist columns (George et al., 2023; Janssens et al., 2024), consistent with strong correlations between observed mesoscale vertical velocity and cloudiness (George et al., 2021; Vogel et al., 2022). Representing SMOCs and their co-variability with moisture in models is therefore a crucial step toward capturing mesoscale cloud organization and improving climate predictions.

Coarse-resolution global climate models with a grid spacing of around 100 km (Balaji et al., 2018) cannot explicitly resolve the SMOCs. Moreover, these circulations are not represented in their cloud parameterizations (Vogel et al., 2022), which were developed without accounting for contributions from mesoscale motions

(George et al., 2023; Vogel et al., 2022). Recently, multi-decadal simulations with 10 km grid spacing under a Shared Socioeconomic Pathway (SSP) scenario have been produced using Earth system models for the first time (Segura et al., 2025), representing a major achievement and motivating our study that uses these data sets. The ICOsahedral Nonhydrostatic (ICON) model adopts a minimalist approach (Hohenegger et al., 2023), whereas the Integrated Forecasting System (IFS) model incorporates many years of model tuning to produce accurate weather forecasts and employs a full range of sophisticated parameterization schemes (ECMWF, 2023; Rackow et al., 2025). Despite these distinct strategies, the overall performance of ICON and IFS regarding trade-wind cumuli is comparable, with both models properly capturing the annual cycle (Nowak et al., 2025).

Despite these advances in kilometer-scale global modeling, some studies suggest that representing the cloud–circulation coupling of trade cumuli requires resolution spanning from the synoptic down to the hectometer (Janssens et al., 2024; Matheou et al., 2011; Nowak et al., 2025; Radtke et al., 2021). Consistently, Schär et al. (2020) found that mesoscale organized cloud structures in the trades were captured only in a 2 km simulation with explicit convection, while convection-parameterized simulations at 50 and 12 km failed to reproduce them. At kilometer-scale resolutions, thermals of shallow convection are partially resolved. Hence, kilometer-scale models are far below the resolution needed to reliably represent these clouds. In fact, they capture more of the mesoscale dynamics than the clouds themselves (Satoh et al., 2019). However, trade cumuli organize into mesoscale patterns (Stevens et al., 2019), and the more organized patterns have greater potential to generate condensational heating and drive SMOCs (McCoy et al., 2025). More specifically, the SMOCs were captured using limited-area models with a grid spacing of 2.5 km Savazzi et al. (2025) and by realistic large-eddy simulations (LESs) with a 312 m grid spacing (Janssens et al., 2024).

Mesoscale convective heating is a primarily triggering mechanism of SMOCs (Janssens et al., 2024), but its representation depends on smaller-scale processes, including cloud microphysics, coupled air–sea interaction processes, and surface-driven turbulence, all of which rely on parameterization schemes. Both finer grid spacing and parameterization schemes influence the amount and vertical distribution of shallow convective heating, making them important factors controlling SMOCs. For these reasons, it remains uncertain how Earth system models simulate SMOCs.

In this work, we investigate how kilometer-scale Earth system models, with grid spacings from 10 km down to 2.8 km, represent the vertical structure, strength, prevalence, and moisture co-variability of SMOCs. The complementary strategies of the ICON and IFS models allow us to assess the extent to which the simulation fidelity depends on parameterizations and the tuning of remaining unresolved small-scale processes. Additional IFS sensitivity simulations with explicit shallow and deep convection were evaluated to further explore these processes.

2. Materials and Methods

2.1. Observational Data

The observations used were collected during the EUREC^{4}A (ElUcidating the RolE of Clouds Circulation Coupling in Climate) field campaign (Bony et al., 2017; Stevens et al., 2021), which took place in the Atlantic trade-winds region east of Barbados during January and February 2020. The High Altitude and Long Range Research Aircraft (HALO) (Konow et al., 2021) operated at an altitude of about 10 km, primarily following a fixed circular flight path known as the EUREC^{4}A-Circle centered at 13.3°N, 57.7°W, with a diameter of around 200 km (George et al., 2021a; Stevens et al., 2021). HALO flights occurred every 2 days, with most comprising six circles, each lasting 1 hr. The flight strategy was statistical and independent of meteorological conditions. The data set JOANNE (Joint dropsonde Observations of the Atmosphere in tropical North atlaNtic mesoscale Environments) provides measurements from the EUREC^{4}A's HALO dropsondes (George et al., 2021a). We used the JOANNE level-4 data, which offers mesoscale circle-average quantities (George et al., 2021b). The quantities analyzed in this study are the divergence, vertical velocity, and specific humidity. We used data from 11 research flights, totaling 65 circles (George et al., 2023).

2.2. Models and Simulations

The analyzed simulations were developed as part of the next Generation of Earth Modeling Systems (nextGEMS) project using two global kilometer-scale Earth system models, ICON and IFS (Segura et al., 2025). These models

10.1029/2025GL119706

Table 1
Characteristics of the Global Coupled Model Simulations

Model	Δx (km)	Deep-shallow convection	Forcing	Output	Label
ICON	10	off—off	SSP3-7.0	24 hr	ICON-reference
IFS-FESOM	9	RCBMF[a]—on	SSP3-7.0	6 hr	IFS-reference
IFS-FESOM	9	on—on	2020	6 hr	IFS-FESOM-DConSCon
IFS-FESOM	4.4	RCBMF[a]—on	2020	6 hr	IFS-FESOM-DCrcbmfSCon-4 km
IFS-FESOM	2.8	RCBMF[a]—on	2020	6 hr	IFS-FESOM-DCrcbmfSCon-2.8 km
IFS-NEMO	9	on—on	2020	6 hr	IFS-NEMO-DConSCon
IFS-NEMO	9	RCBMF[a]—on	2020	6 hr	IFS-NEMO-DCrcbmfSCon
IFS-NEMO	9	off—on	2020	6 hr	IFS-NEMO-DCoffSCon
IFS-NEMO	9	off—off	2020	6 hr	IFS-NEMO-DCoffSCoff
ICON	5	off—off	2020	6 hr	ICON-5 km

Note. The columns show (from left to right): the atmospheric and ocean model, the approximate horizontal grid spacing of the atmosphere (Δx), the use of deep and shallow convection parameterizations, the radiative forcing, the output frequency of the three-dimensional data, and a simulation label used in figures and categorization. [a]Reduced cloud-base mass flux.

and their configurations are described in detail in recent papers (Hohenegger et al., 2023; Rackow et al., 2025; Segura et al., 2025). Therefore, we present only the relevant information for our study. Regarding the parameterization schemes, ICON minimizes their use in the atmosphere, only including cloud microphysics, radiation, and turbulent mixing (Hohenegger et al., 2023). By contrast, the IFS model employs a full suite of parameterization schemes for radiation, cloud and precipitation microphysics, deep, shallow, and mid-level convection, orographic and non-orographic gravity wave drag, and turbulent mixing (ECMWF, 2023; Rackow et al., 2025).

The main characteristics of the simulations relevant to this work are summarized in Table 1. We analyzed both scenario and sensitivity simulations. The scenario simulations employed the SSP3-7.0 scenario and were produced using both global coupled models: IFS coupled with the Finite-volumE Sea ice-Ocean Model (FESOM), and ICON. We consider these scenario simulations as our reference cases and refer to them as IFS-reference and ICON-reference, respectively (first two rows in Table 1).

In addition, a series of simulations with constant radiative forcing fixed at 2020 levels was conducted to assess the sensitivity of the results to model configuration, primarily with the IFS model. The sensitivity simulations allow us to isolate the influence of the ocean component, convection parameterizations, and grid spacing (rows 3 to 10 in Table 1). The sensitivity of the IFS model to the convection parameterizations was investigated by comparing different IFS simulations coupled with the Nucleus for European Modeling of the Ocean model (NEMO), which considered fully active or disabled deep and shallow convection parameterizations, as well as deep convection with reduced cloud-base mass flux (RCBMF), meaning that the mass flux in the convective closure is reduced by a factor of 6. The RCBMF was introduced in the IFS model to increase the fraction of resolved deep convection and to intensify precipitation (Rackow et al., 2025; Segura et al., 2025; Takasuka et al., 2026).

The simulations aligned with the EUREC^{4}A campaign were initialized in January 2020. With the exception of the ICON-reference and the IFS sensitivity run with 2.8 km grid spacing, which were initialized on 1 January 2020, the other simulations were initialized on 20 January 2020.

2.3. Analysis Methods

To assess the realism of the simulations in representing SMOCs, we used the JOANNE data set (Section 2.1) and the ECMWF Reanalysis v5 (ERA5) (Hersbach et al., 2020), which capture mesoscale divergence patterns observed during the EUREC^{4}A campaign (George et al., 2023). Regarding divergence in ERA5, we used the output variable directly, and there was no need to compute it. ERA5 and the global coupled models have six-hourly output (00, 06, 12, and 18 UTC), except for ICON-reference, which has daily output at 00 UTC (Table 1).

The Earth system model simulations analyzed are fully coupled and free-running, with the ocean component requiring a longer spin-up time (Rackow et al., 2025; Segura et al., 2025). Because the simulations were initialized at the start of the EUREC^{4}A campaign, a short-term, time-matched comparison with observations might initially seem preferable to a climatological comparison (Nowak et al., 2025). However, restricting the analysis to such a short period would substantially reduce the sample size and limit the statistical robustness of the comparison. Therefore, we adopt a longer-term analysis approach and compare the simulations with ERA5 to assess their realism, following previous studies (Dolores-Tesillos et al., 2025; Kuma et al., 2025; Nowak et al., 2025; Rackow et al., 2025; Segura et al., 2025; Wille et al., 2025). A comparison with the EUREC^{4}A campaign observations remains useful to assess the order of magnitude and vertical structure of the variables, providing insight into whether the models capture the correct mesoscale structure of SMOCs.

For all data sets, we analyzed the campaign months (January and February). For the Earth system model simulations, output from the first six simulated years (2020–2025) was included for the reference simulations (IFS-reference and ICON-reference), following Segura et al. (2025). During this period, SSP3-7.0 forcings had a limited impact, with the global mean near-surface temperature changing from 2020 to 2025 by +0.5 K in IFS and −0.2 K in ICON. Detailed temperature trends are described in Segura et al. (2025). Data from the first two simulated years (2020–2021) were included for the IFS and ICON sensitivity runs using finer grid spacing (4.4 and 2.8 km for IFS, and 5 km for ICON), and data from 2020, the only year available, were considered for the 9 km sensitivity simulations. For ERA5, we considered the period 2010–2023 (Kluft, 2023).

The simulation output from the global coupled models and ERA5 were averaged over the grid points within the EUREC^{4}A-Circle to ensure consistency with the observations (George et al., 2023), which represent a mesoscale circle average (George et al., 2021a). The simulated vertical velocity averaged over the EUREC^{4}A-Circle was converted to horizontal divergence using mass conservation and the Boussinesq approximation (Bony & Stevens, 2019; Janssens et al., 2024), applying second-order central differences.

The simulated quantities analyzed in this study are divergence, vertical velocity, specific humidity, and cloud liquid water content (q_c). Cloud liquid water is a crucial variable because it affects albedo, which in turn influences climate radiative feedbacks, and it is related to the amount of convective heating realized, which controls the strength of the SMOCs (Janssens et al., 2024). The q_c is typically overestimated by ICON in regions of marine low-level clouds (Nowak et al., 2025). A cloud inhomogeneity factor is therefore used to scale down the ICON q_c before calculating the shortwave fluxes, thereby tuning the radiation balance (Segura et al., 2025). Following Nowak et al. (2025), we introduced the radiatively active q_c*, defined as q_c multiplied by the inhomogeneity factor. This factor is a function of lower-tropospheric stability for the ICON-reference run, whereas it is fixed at 0.4 for the ICON-5 km sensitivity simulation. Here, for simplicity, we applied a cloud inhomogeneity factor of 0.4 to the q_c from both ICON simulations and the value of 1 for the IFS simulations.

To quantify mesoscale circulation characteristics, SMOC strength and prevalence were estimated for the global coupled models, ERA5, and JOANNE. We identify a SMOC event when a dipole is present, that is, when the sub-cloud $\left(D'_{\text{sc}}\right)$ and cloud-layer $\left(D'_{\text{c}}\right)$ mesoscale divergence anomalies have opposite signs (George et al., 2023) and whose magnitude exceed $10^{-6}\ \text{s}^{-1}$ (Savazzi et al., 2025). Following Savazzi et al. (2025), the SMOC strength is defined as the magnitude of this dipole, $|D'_{\text{c}} - D'_{\text{sc}}|$, while the sign of the sub-cloud layer divergence defines mesoscale ascent $\left(D'_{\text{sc}} < 0\right)$ and mesoscale descent $\left(D'_{\text{sc}} > 0\right)$. Here, these metrics are applied to divergence anomalies (George et al., 2023) and the results are shown in Figure 2.

3. Results

3.1. Assessment of the Reference Simulations

For clarity in interpreting the results, the terms sub-cloud layer, cloud-base layer, and cloud layer are used to broadly denote altitude intervals of 0–600 m, 600–900 m, and 900–1,500 m above the surface, respectively, following George et al. (2023).

To investigate the vertical variability of SMOCs and their co-variability with moisture, vertical profiles were composited according to sub-cloud layer divergence quartiles (George et al., 2023; Janssens et al., 2024). The results are shown in Figure 1 for the reference simulations, and in the Supporting Information (Figures S3 and S4 in Supporting Information S1) for the sensitivity simulations. The lowest quartile (Q1), comprising the first 25% of the data, corresponds to cases with stronger convergence in the sub-cloud layer. In contrast, the highest quartile (Q4), comprising the top 25%, corresponds to cases with stronger positive divergence.

10.1029/2025GL119706

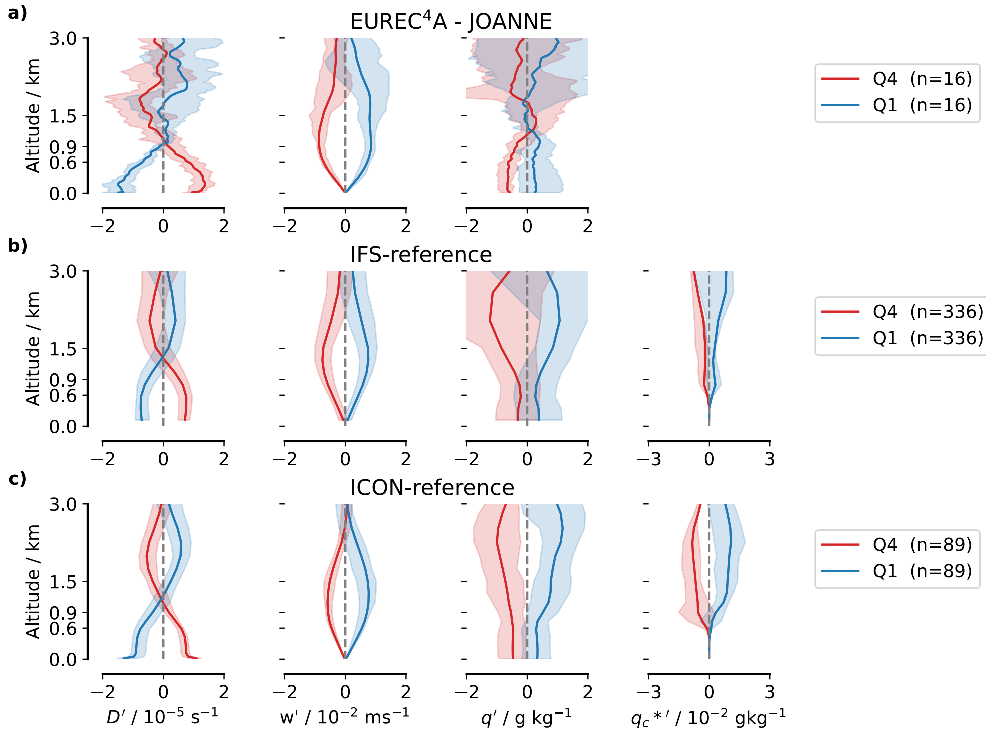

Figure 1. Averaged profiles of anomalies of divergence, vertical velocity, specific humidity, and radiatively active cloud liquid water content (from left to right) are shown for the lowest (Q1, strongest convergence, blue) and highest (Q4, strongest divergence, red) quartiles of divergence in the sub-cloud layer. The shading shows the interquartile range (IQR) for Q1 and Q4. Sample sizes are provided in parentheses in the legends. JOANNE observations (a), IFS-reference simulation (b), and ICON-reference simulation (c), are shown.

Figure 1 highlights the consistency in both depth and magnitude of the divergence and vertical velocity anomalies between EUREC^{4}A observations and the simulations, and the clear separation of the quartiles. The simulations capture the ascending branch of the circulations (first quartile), with a convergence anomaly in the sub-cloud layer and a positive divergence anomaly in the cloud layer. The descending branch (fourth quartile) is also represented, with a positive divergence anomaly in the sub-cloud layer and a convergence anomaly above the cloud base. Consistent with observations (Figure 1a), these divergence anomalies form a dipole, indicating the occurrence of SMOCs (George et al., 2023).

Regarding the anomalies of specific humidity and radiatively active cloud liquid water content (q_c*'; see definition in Section 2.2), both reference simulations show well-separated quartiles throughout the column (Figures 1b and 1c). The anomalously moister profiles of humidity and cloud liquid water occur in the ascending branch of the circulations, while the descending branch features anomalously drier profiles. This co-variability of the SMOCs with humidity (George et al., 2023) is consistent with the observations (Figure 1a) and indicates that the simulations realistically represent SMOCs and their driving mechanisms, similar to LESs with much higher resolution (Janssens et al., 2024).

Although the overall magnitude of the anomalies is comparable, the simulations exhibit peak divergence anomalies of similar strength in both the sub-cloud layer and above the cloud layer (Figures 1b and 1c), whereas the observations show stronger divergence anomalies in the sub-cloud layer (Figure 1a). For humidity, the simulations overestimate anomalies in and above the cloud layer and underestimate them in the sub-cloud layer. This misrepresentation of mesoscale humidity anomalies is also present in LESs with a 312 m grid spacing (Janssens et al., 2024). However, it should be noted that the reference simulations represent a 6-year average over January and February (2020–2025), whereas the observations represent only a single year (January–February 2020; Section 2.3).

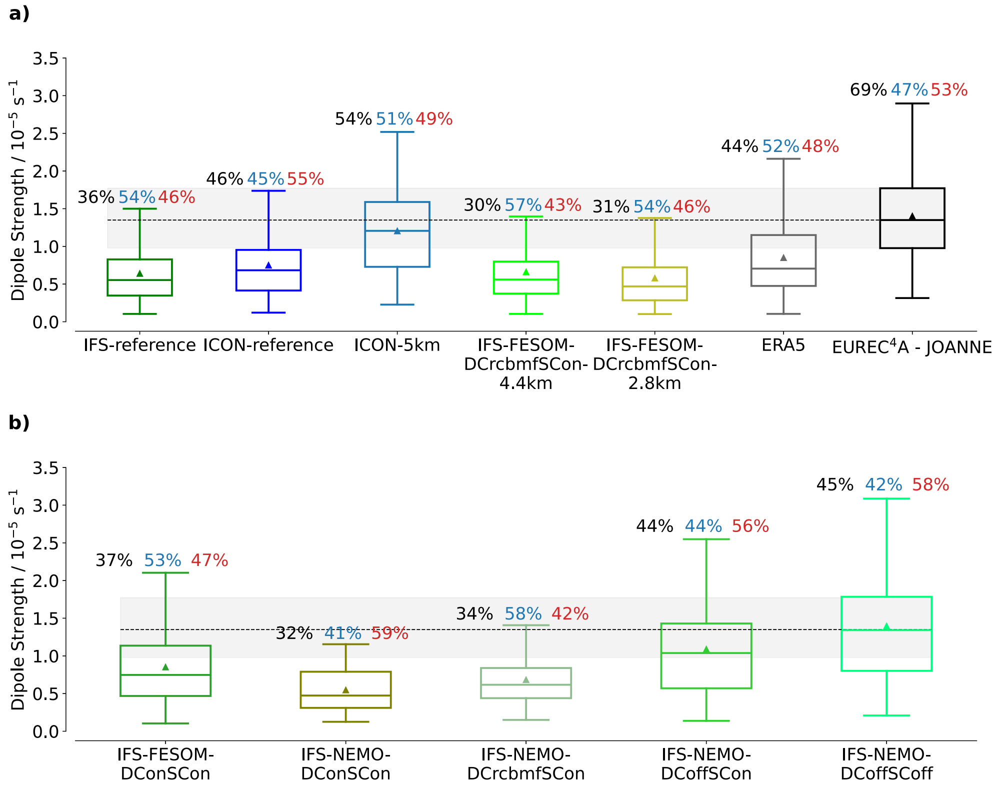

Figure 2. Distribution of SMOC strength, defined as the magnitude of the dipole (i.e., the difference between the divergence anomaly in the cloud layer and that in the sub-cloud layer). Only SMOC events are included in this distribution. Boxes indicate the interquartile range, with the central line marking the median and the triangle denoting the mean. Percentages above each box show the fraction of time SMOC events occur (black) and those associated with mesoscale ascent (blue) or descent (red). (a) Reference simulations, ERA5, and ICON high-resolution run at 00 UTC, IFS high-resolution runs with six-hourly output, and JOANNE observations; (b) IFS model sensitivity simulations with six-hourly output. For all panels (a–b), January and February are considered. The JOANNE data set median (dashed line) and interquartile range (shaded area) are shown for comparison. The periods analyzed for each data set are detailed in Section 2.3.

Dipole strength and prevalence were estimated to quantify SMOC characteristics (Section 2.3). ERA5 captures observed divergence patterns (George et al., 2023), and a long-term data set is available. Therefore, it might initially seem preferable to use ERA5 long-term rather than the JOANNE observational data for 2020 to assess the realism of the simulations. Nevertheless, SMOC strength and occurrence in ERA5 are considerably underestimated compared to JOANNE (Figure 2a), even when considering only the EUREC^{4}A campaign period (Figure S1a in Supporting Information S1). Consequently, comparisons of the dipole strength distributions and number of SMOC occurrences among ERA5, JOANNE, and the simulations should be interpreted with caution.

Both reference simulations exhibit a weaker distribution of dipole strength compared to ERA5, and this difference is even more pronounced compared to JOANNE (Figure 2a). Relative to ERA5, the reference simulations reproduce roughly the same number of SMOC occurrences, although 8% fewer are captured in IFS-reference. Compared to JOANNE, ICON-reference reproduces 23% fewer SMOC occurrences, whereas IFS-reference underestimates them by 33%. The sign of the divergence anomaly in the sub-cloud layer indicates mesoscale ascent when negative and mesoscale descent when positive (Section 2.3). Across all data sets, the numbers of mesoscale ascents and descents are nearly balanced. However, these counts alone do not capture the amplitude and distribution of the extremes. Nevertheless, skewness provides a more direct, quantitative measure of distributional asymmetry and the relative contribution of extreme values.

Shallow cumulus regions are characterized by narrow, strong updrafts compensated by broad, weak downdrafts, which typically produces a positive skewness in sub-cloud layer vertical velocity (Jeong et al., 2022; Klingebiel et al., 2021; Zhu & Zuidema, 2009). The computed skewness of the sub-cloud layer mesoscale vertical velocity anomaly $\left(w'_{\mathrm{sc}}\right)$ is close to zero in JOANNE observations and ERA5, indicating nearly symmetric distributions at these scales (Table S1 in Supporting Information S1). While IFS-reference shows a larger fraction of mesoscale ascent than descent occurrences and near-zero (slightly negative) skewness, ICON-reference exhibits a larger fraction of descent than ascent occurrences and stronger positive skewness (0.72). This overall agreement between the two measures suggests that the differences in ascent/descent fractions among simulations reflect differences in the asymmetry of the w'_{sc} distribution. This relationship is further discussed in Section 3.2.2, where the role of convection parameterizations is examined.

3.2. Sensitivity of IFS to Model Configuration

3.2.1. Ocean Model

Because the surface fluxes that drive boundary-layer thermals strongly depend on sea surface temperature (SST), we investigate how the ocean component of the IFS model shapes SST mean state and variability and how this, in turn, may affect the representation of SMOCs. To this end, we compared the IFS sensitivity simulations coupled with FESOM and NEMO (third and sixth rows in Table 1, respectively), which differ only in their ocean component. In terms of configuration, NEMO is the model used in the ECMWF numerical weather prediction system, performing data assimilation on a 0.25° resolution grid. FESOM employs a grid spacing of around 13 km in the tropics, allowing for the representation of finer ocean structures. The initialization also differed: NEMO was initialized at the start of the simulation on 20 January 2020, whereas FESOM spun up in stand-alone mode for 5 years prior to the simulation (Rackow et al., 2025).

For the region and period analyzed, the mean SST of IFS-FESOM was about 0.5 K colder than that of IFS-NEMO. Colder SSTs are related to more organized shallow cumuli, which have greater potential to generate mesoscale condensational heating and drive SMOCs (McCoy et al., 2025). Another mechanism involves SST heterogeneity: the higher-resolution grid of IFS-FESOM captures stronger mesoscale SST variability (average standard deviation of anomalies 0.38°C, 75th percentile 0.24°C) compared to IFS-NEMO (0.26°C, 0.16°C). Stronger SST gradients modulate surface fluxes, driving buoyancy-driven atmospheric turbulence and near cloud-base cloudiness, and represent another pathway through which mesoscale variability can arise, potentially seeding SMOCs (Chen et al., 2023, 2025). Beyond these ocean-to-atmosphere effects, air-sea interaction feedbacks also play a role (Schmitt et al., 2025).

Whether through colder mean SST or stronger SST variability, both factors favor the development of SMOCs in IFS-FESOM. Our findings confirm this: IFS-FESOM captures stronger SMOCs and 5% more SMOC occurrences than IFS-NEMO (Figure 2b), in closer agreement with JOANNE observations. Nevertheless, the quartile anomaly profiles are similar between the two simulations (Figure S3a in Supporting Information S1).

3.2.2. Parameterized Convection

In this section, we investigate how shallow and deep convection parameterization schemes influence the SMOCs representation on the IFS-NEMO sensitivity simulations. The vertical transport of heat, momentum, and moisture by parameterized shallow convection has been shown to strongly control SMOCs (Savazzi et al., 2025). By contrast, deep convection during boreal winter is expected to exert only a limited indirect influence on the trade-wind region, where SMOCs are ubiquitous.

The influence of deep convection is systematic: reducing the cloud-base mass flux and subsequently disabling the deep convection scheme, incrementally increases SMOC strength and occurrence compared to the simulation with the deep convection scheme fully active (Figure 2b). The stronger distribution of SMOCs strength and occurrence is in closer agreement with JOANNE observations. Given the expected limited influence of deep convection, this result is noteworthy.

One possible pathway is through the acceleration of the Hadley circulation when the deep convection scheme is disabled (Clark et al., 2024), which could lead to enhanced subsidence in the trade-wind region, increased low-tropospheric stability, and a larger shallow cumulus cloud fraction (Mieslinger et al., 2019). Increased low-tropospheric stability is related to more organized shallow cumuli (Bony et al., 2020), which have greater potential to generate mesoscale condensational heating and drive SMOCs (McCoy et al., 2025). Our results indicate that disabling deep convection parameterization is linked to enhanced subsidence and warming above 2 km, stabilizing the lower troposphere (Figure S7 in Supporting Information S1). As emphasized by McCoy et al. (2025), observational evidence suggests that additional assessment of how environmental factors influence mesoscale cloud organization is warranted.

Disabling the shallow convection parameterization further intensified the SMOCs (rightmost box plot in Figure 2b), in closer agreement with JOANNE observations. While the SMOCs strengthened, disabling the shallow convection scheme reduced humidity anomalies in the sub-cloud layer, indicating that the well separated humidity anomaly quartiles throughout the column originate from the shallow-convection parameterization rather than from an explicit representation (Figure S3c in Supporting Information S1). The shallow convection parameterization scheme in IFS represents both updrafts and downdrafts. The downdraft mass flux is considered proportional to the updraft mass flux. At the level of free sinking, the downdraft is defined to have 30% of the strength that the updraft has at cloud base (ECMWF, 2023). The deep convection scheme follows the same definition. Compared to the effect of the ocean component (Section 3.2.1), the impact of convection parameterizations was larger (Figure 2b).

Our findings regarding the shallow convection parameterization are consistent with Savazzi et al. (2025), who found that disabling this scheme increased the strength of SMOCs in limited-area simulations using the HARMONIE-AROME model with a grid spacing of 2.5 km. Our computed time-mean profiles show that when shallow convection is disabled, the sub-cloud layer becomes moister, the cloud layer drier, and more unstable (Figure S7 in Supporting Information S1). These results agree with the impact of shallow convection scheme on the average profiles shown by Savazzi et al. (2025), who attributed the change in moisture to vertical mixing. When shallow convection is turned off, resolved eddies transport heat and moisture more efficiently within the cloud layer, while the sub-cloud layer is less well mixed. This increases instability and strengthens resolved updrafts.

These dynamical changes are also reflected in the statistical properties of w'_{sc} (Table S1 in Supporting Information S1). IFS simulations with active shallow convection parameterization show skewness values of w'_{sc} close to zero and generally correspond to a larger fraction of detected mesoscale ascents than of descents. Conversely, simulations with disabled convection parameterizations (i.e., the IFS-NEMO-DCoffSCon and IFS-NEMO-DCoffSCoff runs, as well as both ICON runs) exhibit stronger positive skewness values and generally correspond to a smaller fraction of detected mesoscale ascents than of descents. This suggests that strong, narrow updrafts become more pronounced when convection parameterizations are disabled, consistent with Savazzi et al. (2025). These stronger updrafts are more likely to reach the condensation level, release latent heat, and thereby favor SMOC development (Janssens et al., 2024; McCoy et al., 2025).

To account for the relationship between SMOCs and clouds (Janssens et al., 2024; McCoy et al., 2025; Savazzi et al., 2025), the data sets were split by mesoscale cloud cover within the EUREC^{4}A-Circle (Text S1 in Supporting Information S1). Although the results for dipole strength (Figure S2 in Supporting Information S1) remain qualitatively consistent with those obtained without conditioning on cloud cover (Figure 2), a cloud-conditioned behavior of sub-cloud layer mesoscale ascents and descents is evident. In simulations with active parameterized shallow convection, the fraction of mesoscale ascent occurrences is higher in low mesoscale cloud-cover cases than in high cloud-cover cases. In contrast, for simulations with the shallow convection parameterization disabled, the opposite behavior is found: the fraction of mesoscale ascents increases markedly from 14% and 37% in low-cloud-cover cases to 69% and 65% in high-cloud-cover cases for IFS–NEMO–DCoffSCoff and ICON-5 km, respectively. A complementary decrease in mesoscale descent occurrences is found across these conditions. These results suggest that conditioning on cloud cover modulates the fraction of mesoscale ascent occurrences, and that the relationship depends on the treatment of shallow convection parameterization.

3.3. ICON and IFS Simulations Using Smaller Grid Spacing

We also investigate simulations with finer grid spacings of 2.8 and 4.4 km for IFS-FESOM and 5 km for ICON (Figure 2c). Given that the 9–10 km simulations (Sections 3.1 and 3.2) reproduced key features of the SMOCs and their co-variability with moisture, as expected, the finer resolution runs also captured these features (Figures S4a and S4b in Supporting Information S1). Because SMOCs have typical horizontal scales on the order of 100 km, one might initially expect that reducing the grid spacing below 10 km would have a limited impact. However, trade cumuli organize into mesoscale patterns (Stevens et al., 2019), and the more organized patterns have greater potential to generate condensational heating and drive SMOCs (McCoy et al., 2025). Within this resolution range,

10.1029/2025GL119706

trade-wind mesoscale organized cloud structures were captured only in a 2 km simulation with explicit convection, while convection-parameterized simulations at 12 km failed to reproduce them (Schär et al., 2020). At kilometer-scale resolutions, thermals of shallow convection are partially resolved, so finer grid spacing may influence the amount and vertical distribution of shallow convective heating. Therefore, this motivates our investigation of the influence of horizontal resolution on SMOC strength and prevalence.

The influence of grid spacing cannot be isolated for the ICON 5 km run because of several configuration differences between the lower- and higher-resolution runs, as detailed by Segura et al. (2025). Nevertheless, the finer-resolution simulation exhibited substantial increased SMOC strength an 8% higher occurrence compared to the ICON-reference run (Figure 2a), providing useful insights into the sensitivity of the simulated SMOCs to model configuration. For IFS-FESOM, reducing the horizontal grid spacing slightly weakened the SMOCs and reduced their occurrence (Figure 2a). Compared to the effect of convection parameterizations (Section 3.2.2), the impact of resolution was smaller.

4. Conclusions

A key step in model development is the validation of model results against observations. This study analyzed ICON and IFS Earth system model simulations with grid spacings from 10 km down to 2.8 km to assess their ability to represent the vertical structure, strength, prevalence, and moisture co-variability of SMOCs. For this purpose, EUREC^{4}A campaign and ERA5 data were used. We examined scenario runs as reference simulations, over the period 2020–2025, and also analyzed sensitivity simulations with a constant 2020 radiative forcing to evaluate the impact of different model configurations on SMOCs.

Vertical profiles of atmospheric anomaly variables were composited based on quartiles of sub-cloud layer divergence (following George et al. (2023)). The depth and magnitude of the divergence and vertical velocity anomalies, as well as the clear separation of the quartiles, are highly consistent between EUREC^{4}A campaign observations and the reference simulations. In agreement with the observations, the reference simulations with 10 km grid spacing captured divergence anomalies characterized by sign reversals between the sub-cloud and cloud layers, forming a dipole structure, indicative of SMOCs occurrence (George et al., 2023).

Regarding moisture co-variability, anomalously drier profiles in the simulations occur in the descending branch of the circulations, while the ascending branch exhibits anomalously moister profiles, consistent with observations (George et al., 2023), and indicating that the simulations realistically represent SMOCs and their triggering mechanisms. However, while the humidity anomaly is overestimated by the simulations in the cloud layer, it is underestimated in the sub-cloud layer. A similar underestimation of mesoscale humidity anomalies was also found in LESs with hectometer-scale grid spacings (Janssens et al., 2024).

Additionally, IFS simulations provided further insight into the sensitivity of the model configuration. The comparison revealed that (a) switching from the NEMO to the FESOM ocean model, (b) disabling deep, and (c) shallow convection parameterization schemes enhanced SMOCs and increased their occurrence, bringing the simulations into closer agreement with JOANNE observations. Compared to the effect of the ocean component, the impact of convection parameterizations was larger. The deep convection scheme had a large impact on the circulation, an important insight given the indirect (and typically assumed limited) influence of deep convection in the trade-wind region where SMOCs are ubiquitous. Regarding horizontal resolution, reducing grid spacing in IFS slightly weakened the SMOCs, whereas in ICON it tends to strengthen them.

These dynamical changes are also reflected in the statistical properties of the sub-cloud layer mesoscale vertical velocity anomaly. IFS simulations with active shallow convection parameterization show skewness values close to zero and generally exhibit a larger fraction of detected mesoscale ascents than of descents. In contrast, ICON and IFS simulations with the shallow convection parameterization disabled display stronger positive skewness and generally exhibit a smaller fraction of detected mesoscale ascents than of descents. This suggests that strong, narrow updrafts become more pronounced when convection parameterizations are disabled, consistent with Savazzi et al. (2025).

Although the results for dipole strength conditioned on cloud-cover remain qualitatively consistent with those obtained without conditioning, a cloud-conditioned behavior of mesoscale ascents and descents is nevertheless evident, and this relationship depends on the treatment of convection. For ICON and IFS simulations with the shallow convection parameterization disabled, the fraction of mesoscale ascents increases markedly in mesoscale high-cloud-cover cases relative to low-cloud-cover cases. A complementary decrease in mesoscale descent occurrences is found across these conditions.

Overall, this study demonstrates that global coupled models with grid spacings of 2.8–10 km can capture the key characteristics of SMOCs and their co-variability with moisture. We show that these representations are sensitive to convection parameterizations, ocean models, and horizontal resolution, providing guidance on the relative importance of each of these factors. Accurately representing SMOCs and their co-variability with moisture in models is therefore a crucial step toward capturing mesoscale cloud organization and improving climate predictions.

Conflict of Interest

The authors declare no conflicts of interest relevant to this study.

Availability Statement

The simulations are from the nextGEMS project and are openly accessible on the supercomputer Levante of the German Climate Computing Center (DKRZ) after registration at https://luv.dkrz.de/register/. ERA5 data obtained from DKRZ (Kluft, 2023) were used. The EUREC^{4}A observations were taken from the JOANNE level-4 data set publicly available (George et al., 2021b). The Python code developed for our analysis is publicly available in the repository Dragaud (2025).

Acknowledgments
This research was supported by the EU Horizon 2020 project nextGEMS under Grant Agreement Number 101003470, and the Cluster of Excellence Climate, Climatic Change, and Society (CLICCS, EXC 2037), funded by the German Research Foundation (DFG) under Germany's Excellence Strategy. Raphaela Vogel acknowledges support from an ERC starting grant (ROTOR, Grant 101116282). We acknowledge financial support from the Open Access Publication Fund of Universität Hamburg. The data analysis for this work was performed using the Levante supercomputer at the German Climate Computing Center (DKRZ), using DKRZ resources granted by its Scientific Steering Committee (WLA) under project IDs bb1153 and bm1235. The authors thank Geet George for sharing his insights, which contributed to the development of this paper. We acknowledge the collective efforts of both the EUREC^{4}A and nextGEMS teams in the collection and processing of the data. We thank the two anonymous reviewers for their constructive comments and insightful suggestions, which greatly improved the clarity and quality of this manuscript. Open Access funding enabled and organized by Projekt DEAL.

References

Balaji, V., Taylor, K. E., Juckes, M., Lawrence, B. N., Durack, P. J., Lautenschlager, M., et al. (2018). Requirements for a global data infrastructure in support of CMIP6. *Geoscientific Model Development*, *11*(9), 3659–3680. https://doi.org/10.5194/gmd-11-3659-2018

Bony, S., Poujol, B., McKim, B., Rochetin, N., Lothon, M., Windmiller, J., et al. (2025). Evidence for the role of thermal and cloud merging in mesoscale convective organization. *Atmospheric Chemistry and Physics*, *25*(23), 17331–17362. https://doi.org/10.5194/acp-25-17331-2025

Bony, S., Schulz, H., Vial, J., & Stevens, B. (2020). Sugar, gravel, fish, and flowers: Dependence of mesoscale patterns of trade-wind clouds on environmental conditions. *Geophysical Research Letters*, *47*(7), e2019GL085988. https://doi.org/10.1029/2019gl085988

Bony, S., & Stevens, B. (2019). Measuring area-averaged vertical motions with dropsondes. *Journal of the Atmospheric Sciences*, *76*(3), 767–783. https://doi.org/10.1175/jas-d-18-0141.1

Bony, S., Stevens, B., Ament, F., Bigorre, S., Chazette, P., Crewell, S., et al. (2017). EUREC4A: A field campaign to elucidate the couplings between clouds, convection and circulation. *Surveys in Geophysics*, *38*(6), 1529–1568. https://doi.org/10.1007/s10712-017-9428-0

Chen, X., Dias, J., Wolding, B., Blossey, P. N., DeMott, C., Pincus, R., & Thompson, E. J. (2025). Impacts of weak sea surface temperature warm anomalies on local trade cumulus cloudiness in large eddy simulations. *Journal of Advances in Modeling Earth Systems*, *17*(7), e2024MS004778. https://doi.org/10.1029/2024ms004778

Chen, X., Dias, J., Wolding, B., Pincus, R., DeMott, C., Wick, G., et al. (2023). Ubiquitous sea surface temperature anomalies increase spatial heterogeneity of trade wind cloudiness on daily time scale. *Journal of the Atmospheric Sciences*, *80*(12), 2969–2987. https://doi.org/10.1175/jas-d-23-0075.1

Clark, J. P., Lin, P., & Hill, S. A. (2024). Itcz response to disabling parameterized convection in global fixed-SST GFDL-AM4 aquaplanet simulations at 50 and 6 km resolutions. *Journal of Advances in Modeling Earth Systems*, *16*(6), e2023MS003968. https://doi.org/10.1029/2023ms003968

Dolores-Tesillos, E., Martius, O., & Quinting, J. (2025). On the role of moist and dry processes in atmospheric blocking biases in the Euro-Atlantic region in CMIP6. *Weather and Climate Dynamics*, *6*(2), 471–487. https://doi.org/10.5194/wcd-6-471-2025

Dragaud, I. (2025). Simulating shallow mesoscale overturning circulations in the trades with kilometer-scale Earth system models: Python software. https://doi.org/10.5281/zenodo.17237583

ECMWF. (2023). *Ifs documentation CY48R1—Part IV: Physical processes*. Author. https://doi.org/10.21957/02054f0fbf

George, G., Stevens, B., Bony, S., Klingebiel, M., & Vogel, R. (2021). Observed impact of meso-scale vertical motion on cloudiness. *Journal of the Atmospheric Sciences*. https://doi.org/10.1175/jas-d-20-0335.1

George, G., Stevens, B., Bony, S., Pincus, R., Fairall, C., Schulz, H., et al. (2021a). Joanne: Joint dropsonde observations of the atmosphere in tropical north Atlantic meso-scale environments. *Earth System Science Data*, *13*(11), 5253–5272. https://doi.org/10.5194/essd-13-5253-2021

George, G., Stevens, B., Bony, S., Pincus, R., Fairall, C., Schulz, H., et al. (2021b). *Joanne: Joint dropsonde observations of the atmosphere in tropical north Atlantic meso-scale environments (v2.0.0)*. AERIS. https://doi.org/10.25326/246

George, G., Stevens, B., Bony, S., Vogel, R., & Naumann, A. K. (2023). Widespread shallow mesoscale circulations observed in the trades. *Nature Geoscience*, *16*(7), 584–589. https://doi.org/10.1038/s41561-023-01215-1

Hersbach, H., Bell, B., Berrisford, P., Hirahara, S., Horányi, A., Muñoz-Sabater, J., et al. (2020). The ERA5 global reanalysis. *Quarterly Journal of the Royal Meteorological Society*, *146*(730), 1999–2049. https://doi.org/10.1002/qj.3803

Hohenegger, C., Korn, P., Linardakis, L., Redler, R., Schnur, R., Adamidis, P., et al. (2023). Icon-sapphire: Simulating the components of the Earth system and their interactions at kilometer and subkilometer scales. *Geoscientific Model Development*, *16*(2), 779–811. https://doi.org/10.5194/gmd-16-779-2023

Janssens, M., George, G., Schulz, H., Couvreux, F., & Bouniol, D. (2024). Shallow convective heating in weak temperature gradient balance explains mesoscale vertical motions in the trades. *Journal of Geophysical Research: Atmospheres*, *129*(18), e2024JD041417. https://doi.org/10.1029/2024jd041417

Jeong, J., Witte, M. K., Glenn, I. B., Smalley, M., Lebsock, M. D., Lamer, K., & Zhu, Z. (2022). Distinct dynamical and structural properties of marine stratocumulus and shallow cumulus clouds in the eastern North Atlantic. *Journal of Geophysical Research: Atmospheres*, *127*(19), e2022JD037021. https://doi.org/10.1029/2022jd037021

Klingebiel, M., Konow, H., & Stevens, B. (2021). Measuring shallow convective mass flux profiles in the trade wind region. *Journal of the Atmospheric Sciences*, *78*(10), 3205–3214. https://doi.org/10.1175/jas-d-20-0347.1

Kluft, L. (2023). ERA5 data on the HEALPIX grid [Dataset]. Retrieved from https://orcestra-campaign.org/hera5.html

Konow, H., Ewald, F., George, G., Jacob, M., Klingebiel, M., Kölling, T., et al. (2021). EUREC4A's halo. *Earth System Science Data*, *13*(12), 5545–5563. https://doi.org/10.5194/essd-13-5545-2021

Kuma, P., Bender, F. A., McDonald, A. J., Alexander, S. P., McFarquhar, G. M., Cassano, J. J., et al. (2025). Ship-based LiDAR evaluation of southern ocean low clouds in the storm-resolving general circulation model icon and the ERA5 and MERRA-2 reanalyses. *Journal of Geophysical Research: Atmospheres*, *130*(22), e2024JD043145. https://doi.org/10.1029/2024jd043145

Matheou, G., Chung, D., Nuijens, L., Stevens, B., & Teixeira, J. (2011). On the fidelity of large-eddy simulation of shallow precipitating cumulus convection. *Monthly Weather Review*, *139*(9), 2918–2939. https://doi.org/10.1175/2011mwr3599.1

McCoy, I. L., Baidar, S., Zuidema, P., Kazil, J., Brewer, W. A., Angevine, W. M., & Feingold, G. (2025). Increased dynamic efficiency in mesoscale organized trade wind cumulus clouds. *Atmospheric Chemistry and Physics*, *25*(22), 16233–16261. https://doi.org/10.5194/acp-25-16233-2025

Mieslinger, T., Horváth, k., Buehler, S. A., & Sakradzija, M. (2019). The dependence of shallow cumulus macrophysical properties on large-scale meteorology as observed in aster imagery. *Journal of Geophysical Research: Atmospheres*, *124*(21), 11477–11505. https://doi.org/10.1029/2019jd030768

Nowak, J. L., Dragaud, I. C. D. V., Lee, J., Dziekan, P., Mellado, J. P., & Stevens, B. (2025). A first look at the global climatology of low-level clouds in storm resolving models. *Journal of Advances in Modeling Earth Systems*, *17*(3), e2024MS004340. https://doi.org/10.1029/2024ms004340

Rackow, T., Pedruzo-Bagazgoitia, X., Becker, T., Milinski, S., Sandu, I., Aguridan, R., et al. (2025). Multi-year simulations at kilometre scale with the integrated forecasting system coupled to FESOM2.5 and NEMOV3.4. *Geoscientific Model Development*, *18*(1), 33–69. https://doi.org/10.5194/gmd-18-33-2025

Radtke, J., Mauritsen, T., & Hohenegger, C. (2021). Shallow cumulus cloud feedback in large eddy simulations—Bridging the gap to storm-resolving models. *Atmospheric Chemistry and Physics*, *21*(5), 3275–3288. https://doi.org/10.5194/acp-21-3275-2021

Satoh, M., Stevens, B., Judt, F., Khairoutdinov, M., Lin, S.-J., Putman, W. M., & Düben, P. (2019). Global cloud-resolving models. *Current Climate Change Reports*, *5*(3), 172–184. https://doi.org/10.1007/s40641-019-00131-0

Savazzi, A. C. M., Nuijens, L., de Rooy, W., & Siebesma, A. P. (2025). The influence of parameterized shallow convection on trade-wind clouds and circulations in the harmonie-arome mesoscale model. *Journal of Advances in Modeling Earth Systems*, *17*(2), e2024MS004538. https://doi.org/10.1029/2024ms004538

Schär, C., Fuhrer, O., Arteaga, A., Ban, N., Charpilloz, C., Di Girolamo, S., et al. (2020). Kilometer-scale climate models: Prospects and challenges. *Bulletin of the American Meteorological Society*, *101*(5), E567–E587. https://doi.org/10.1175/bams-d-18-0167.1

Schmitt, M., Klingbeil, K., Shevchenko, R., & Umlauf, L. (2025). Three-dimensional ocean surface layer response to atmospheric cold pools and diurnal heating in the trade wind regime. *Journal of Geophysical Research: Oceans*, *130*(8), e2024JC022129. https://doi.org/10.1029/2024jc022129

Segura, H., Pedruzo-Bagazgoitia, X., Weiss, P., Müller, S. K., Rackow, T., Lee, J., et al. (2025). nextGEMS: Entering the ERA of kilometer-scale Earth system modeling. *Geoscientific Model Development*, *18*(20), 7735–7761. https://doi.org/10.5194/gmd-18-7735-2025

Stevens, B., Bony, S., Brogniez, H., Hentgen, L., Hohenegger, C., Kiemle, C., et al. (2019). Sugar, gravel, fish and flowers: Mesoscale cloud patterns in the trade winds. *Quarterly Journal of the Royal Meteorological Society*, *146*(726), 141–152. https://doi.org/10.1002/qj.3662

Stevens, B., Bony, S., Farrell, D., Ament, F., Blyth, A., Fairall, C., et al. (2021). EUREC4A. *Earth System Science Data*, *13*(8), 4067–4119. https://doi.org/10.5194/essd-13-4067-2021

Takasuka, D., Becker, T., & Bao, J. (2026). Precipitation characteristics and thermodynamic-convection coupling in global kilometer-scale simulations. *Journal of Advances in Modeling Earth Systems*, *18*(3), e2025MS005343. https://doi.org/10.1029/2025ms005343

Vogel, R., Albright, A. L., Vial, J., George, G., Stevens, B., & Bony, S. (2022). Strong cloud–circulation coupling explains weak trade cumulus feedback. *Nature*, *612*(7941), 696–700. https://doi.org/10.1038/s41586-022-05364-y

Wille, J. D., Koch, R., Becker, T., & Fischer, E. (2025). Extreme precipitation depiction in convection-permitting Earth system models within the nextGEMS project. *Journal of Advances in Modeling Earth Systems*, *17*(7), e2024MS004840. https://doi.org/10.1029/2024ms004840

Zhu, P., & Zuidema, P. (2009). On the use of pdf schemes to parameterize sub-grid clouds. *Geophysical Research Letters*, *36*(5). https://doi.org/10.1029/2008gl036817